MATHEMATICAL BIOSCIENCES
AND ENGINEERING
Volume **4**, Number **4**, October **2007**

http://www.mbejournal.org/

pp. **617–631**

A MODEL OF ACTIVITY-DEPENDENT CHANGES IN DENDRITIC SPINE DENSITY AND SPINE STRUCTURE

S. M. Crook

Department of Mathematics and Statistics and School of Life Sciences,
Arizona State University, Tempe, Arizona 85287

M. Dur-e-Ahmad

Department of Mathematics and Statistics
Arizona State University, Tempe, Arizona 85287

S. M. Baer

Department of Mathematics and Statistics
Arizona State University, Tempe, Arizona 85287

(Communicated by Yang Kuang)

Abstract. Recent evidence indicates that the morphology and density of dendritic spines are regulated during synaptic plasticity. See, for instance, a review by Hayashi and Majewska [9]. In this work, we extend previous modeling studies [27] by combining a model for activity-dependent spine density with one for calcium-mediated spine stem restructuring. The model is based on the standard dimensionless cable equation, which represents the change in the membrane potential in a passive dendrite. Additional equations characterize the change in spine density along the dendrite, the current balance equation for an individual spine head, the change in calcium concentration in the spine head, and the dynamics of spine stem resistance. We use computational studies to investigate the changes in spine density and structure for differing synaptic inputs and demonstrate the effects of these changes on the input-output properties of the dendritic branch. Moderate amounts of high-frequency synaptic activation to dendritic spines result in an increase in spine stem resistance that is correlated with spine stem elongation. In addition, the spine density increases both inside and outside the input region. The model is formulated so that this long-term potentiation-inducing stimulus eventually leads to structural stability. In contrast, a prolonged low-frequency stimulation paradigm that would typically induce long-term depression results in a decrease in stem resistance (correlated with stem shortening) and an eventual decrease in spine density.

1. **Introduction.** Dendritic spines are specialized morphological compartments that are responsible for post-synaptic activity for a vast majority of excitatory synapses in the central nervous system. The number of spines and the spine structure change in response to hormonal signals, synaptic activity, and neurological conditions [22]. For instance, high-frequency stimuli that induce long-term potentiation (LTP), which is presumed to form the cellular basis for learning and memory,

2000 *Mathematics Subject Classification.* 92D30.

Key words and phrases. dendritic spine, dendritic plasticity, long-term potentiation, structural plasticity.

have been associated with increases in the number and size of spines [7, 20]. In contrast, low-frequency stimuli that induce long-term depression (LTD) are associated with decreases in the number and size of spines [22]. Decreases in spine density may also occur due to excitotoxicity associated with very high levels of activity such as during seizures [21, 8, 23]. The time scale of restructuring can range from seconds to hours, and hundreds of spines on a single branch may morph simultaneously but at different rates. Conversely, slow structural changes in spines influence how electrical activity spreads in the cell on a millisecond time scale. Resolving such interactions will improve our understanding of the input-output properties of dendrites and how morphological changes in dendrites both influence and are influenced by electrical and chemical activity in the cell.

The abundance of postsynaptic AMPA receptors, which largely mediate excitatory synaptic transmission, correlates with the number and size of spines [6]. Therefore, the regulation of the formation and morphology of spines is crucial for controlling synaptic strength. Overall, the molecular mechanisms that regulate spines are poorly understood; however, it is now well established that calcium influx is a necessary step in long-term synaptic plasticity [3, 18]. Recent experiments suggest that dendritic spines are unique calcium compartments that regulate local changes in the calcium concentration independently of the parent dendrite [14, 15]. It is suggested that a moderate rise in the calcium concentration may cause elongation of dendritic spines, while a very large increase in calcium concentration may cause fast shrinkage and the eventual collapse of spines [24]. Here we propose a mathematical model based on this conceptual model from [24], and we use computational studies to investigate the changes in spine density and structure for a variety of synaptic inputs of different frequencies and to study the effects of these morphological changes on dendritic output. The model includes activity-dependent spine densities and calcium-restructuring in individual spines and relies on a continuum formulation for the interaction of many spines due to Baer and Rinzel [2].

2. **Model development.**

The model is based on the standard dimensionless cable equation, which is used to model the change in membrane potential in a passive dendrite. An additional equation represents the activity-dependent changes in spine density along the dendrite. For this continuum model, a typical Hodgkin-Huxley current balance equation [11] represents the change in membrane potential in an isopotential compartment representing a spine head. The model also includes an equation for activity-dependent changes in the calcium concentration in spines, as well as an equation for the calcium-mediated changes in spine stem resistance that correspond to changes in spine stem length and structure.

2.1. **Membrane potential along a dendritic branch.**

Consider a branch of passive dendrite cable of length l (μm) with both ends sealed that is studded with a population of dendritic spines. The spine density $\bar{N}$ is defined as the number of spines per unit physical length. Over a short segment Δx, the spine delivers current $\Delta x N I_{ss}$ to the dendrite, where I_{ss} represents the current flowing through an individual spine stem.

As described in [26] and [27], the stem current I_{ss} is expressed as an ohmic voltage drop across the spine stem with resistance R_{ss} ($M\Omega$) and is given by the equation

$$I_{ss} = \frac{V_{sh} - V_d}{R_{ss}} \tag{2.1}$$

where V_{sh} and V_d (mV) are the membrane potentials in the spine head and dendritic base respectively. Previous studies present this simplified model as a good approximation for the neglected membrane and cable properties of the spine stem [25, 2]. Observe that for a very high value of R_{ss}, $I_{ss} \approx 0$ and the spine head is getting very close to isolation from its parent dendrite.

TABLE 1. Parameter values for the calcium-mediated model.

Symbol	Parameter value	Description
A_{sh}	$1.31 \cdot 10^{-8}\ cm^2$	Surface area of each spine head
C_1	$30\ nM$	Lower threshold for calcium in spine
C_2	$300\ nM$	Upper threshold for calcium in spine
C_m	$10^{-3}\ mF/cm^2$	Specific membrane capacitance
C_{min}	$5\ nM$	Calcium lower bound
d	$3.6 \cdot 10^{-5}\ cm$	Dendritic cable diameter
ε_1	$3 \cdot 10^{-3}\ ms^{-1}$	Rate of change in C_a equation
ε_2	$7.5 \cdot 10^{-5}\ ms^{-1}$	Rate of change in R_{ss} equation
ε_3	$1 \cdot 10^{-5}\ ms^{-1}$	Rate of change in $\bar{n}$ equation
γ	2.5	Channel density scale factor
$\bar{g}_{Na}$	$1.2 \cdot 10^{-1}\ S/cm^2$	Maximal sodium conductance
$\bar{g}_K$	$3.6 \cdot 10^{-2}\ S/cm^2$	Maximal potassium conductance
$\bar{g}_L$	$3 \cdot 10^{-4}\ S/cm^2$	Maximal leakage conductance
g_p	$7.4 \cdot 10^{-11}\ S$	Peak synaptic conductance
κ_c	$1 \cdot 10^{-9}\ mA\,ms/nM$	Calcium scale factor
L	3	Dimensionless length of the cable
$\bar{n}_{min}$	16 (≈ 1 spine/$10\mu m$)	Spine density lower bound
$\bar{n}_{max}$	100 (≈ 5 spines/$10\mu m$)	Spine density upper bound
R_i	$70\ \Omega\, cm$	Specific cytoplasmic activity
R_m	$2.5 \cdot 10^3\ \Omega\, cm$	Passive membrane resistance
R_{max}	$1000 \cdot 10^6\ \Omega$	Stem resistance upper bound
R_{min}	$30 \cdot 10^6\ \Omega$	Stem resistance lower bound
R_{sh}	$1.02 \times 10^{11}\ \Omega$	Resistance of each spine head
t_p	$0.2\ ms$	Time to peak for g_{syn}
V_{Na}	$1.15 \cdot 10^2\ mV$	Sodium reversal potential
V_K	$-12\ mV$	Potassium reversal potential
V_L	$10.5989\ mV$	Leakage reversal potential
V_{syn}	$10^2\ mV$	Synaptic reversal potential

The change in electrical potential $V_d(x,t)$ in a passive dendrite studded with $\bar{N}$ spines per unit physical length is given by the cable equation

$$\pi d C_m \frac{\partial V_d}{\partial t} = \frac{\pi d^2}{4R_i}\frac{\partial^2 V_d}{\partial x^2} - \frac{\pi d V_d}{R_m} + \bar{N} I_{ss}. \tag{2.2}$$

Here R_i is the volume resistivity of the cable (measured in Ωcm), R_m is the resistance across the unit area of the passive membrane (measured in Ωcm^2), C_m is the specific membrane capacitance (measured in $\mu F/cm^2$), and d is the diameter of the dendrite (measured in μm). Rewriting the above equation by multiplying by $\frac{R_m}{\pi d}$ gives

$$R_m C_m \frac{\partial V_d}{\partial t} = \frac{d R_m}{4R_i}\frac{\partial^2 V_d}{\partial x^2} - V_d + \frac{\bar{N} I_{ss} R_m}{\pi d}. \tag{2.3}$$

We introduce new parameters $\tau_m = R_m C_m$, $\lambda = \sqrt{\frac{R_m d}{4R_i}}$ and $R_\infty = \frac{R_m}{\pi d \lambda}$ where τ_m is membrane time constant, λ is the length constant and R_∞ is cable input resistance. Using these values in equation (2.3), we get

$$\tau_m \frac{\partial V_d}{\partial t} = \lambda^2 \frac{\partial^2 V_d}{\partial x^2} - V_d + \lambda \bar{N} I_{ss} R_\infty. \tag{2.4}$$

To arrive at the dimensionless cable equation for the electrical potential in the dendrite of dimensionless length $l = L/\lambda$, we make the change of variables $X = x/\lambda$ and $\bar{n} = \lambda \bar{N}$, to get

$$\tau_m \frac{\partial V_d}{\partial t} = \frac{\partial^2 V_d}{\partial X^2} - V_d + \bar{n} I_{ss} R_\infty. \tag{2.5}$$

Here $\bar{n}$ represents the number of spines per unit electronic length λ.

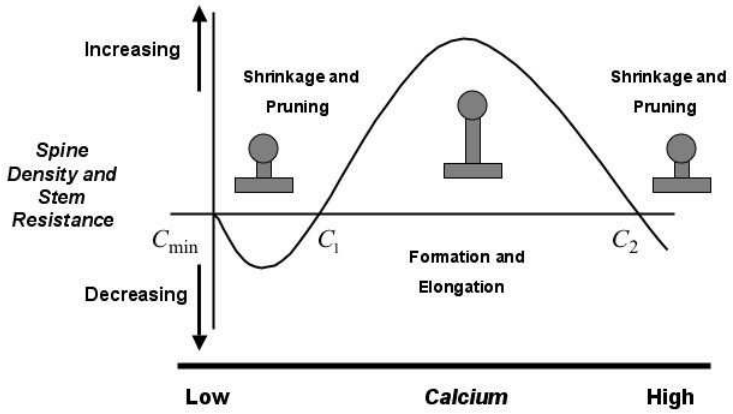

FIGURE 1. Schematic for the conceptual model of the relationship between the calcium concentration and the shape and density of dendritic spines. Low calcium concentrations lead to shrinkage and pruning, an increase in calcium concentration leads to spine elongation and formation of new spines, and significantly higher values cause spine shrinkage and pruning. This conceptual model is adapted from [24].

2.2. **Membrane potential in a spine head.** To model the spine head, we assume that it is an isopotential compartment and let $V_{sh}(x,t)$ denote the membrane potential of the spine head for the population of the spines distributed along the dendrite. The total capacitance on each spine head is calculated by the relation $C_{sh} = A_{sh} C_m$ (μF) where A_{sh} is the spine head surface area and C_m is specific membrane capacitance. The current balance equation for the membrane potential in a single spine is given by

$$C_{sh} \frac{\partial V_{sh}}{\partial t} = -I_{ion} - I_{syn} - I_{ss}. \tag{2.6}$$

Here I_{ion} represents ionic current passing through the head membrane, I_{syn} represents the synaptic current and I_{ss} is the current flowing through the spine stem and is calculated using equation (2.1). For the excitable membrane in the spine head we

use Hodgkin-Huxley kinetics [11] for the voltage dependent ion channel currents. The equation for the ionic current is given by

$$I_{ion} = \gamma A_{sh}[(V_{sh} - V_{N_a})\bar{g}_{N_a} m^3 h + (V_{sh} - V_{_K})\bar{g}_{_K} n^4 + (V_{sh} - V_{_L})\bar{g}_{_L}]. \tag{2.7}$$

Here V_{Na}, $V_{_K}$ and $V_{_L}$ are the reversal potentials for the sodium, potassium, and leakage currents with maximal conductances $\bar{g}_{N_a}$, $\bar{g}_{_K}$ and $\bar{g}_{_L}$ respectively. The activation and inactivation variables m, n and h satisfy the standard first-order equations given by

$$\frac{\partial m}{\partial t} = \alpha_m(1-m) - \beta_m m \tag{2.8}$$

$$\frac{\partial n}{\partial t} = \alpha_n(1-n) - \beta_n n \tag{2.9}$$

$$\frac{\partial h}{\partial t} = \alpha_h(1-h) - \beta_h h \tag{2.10}$$

where

$$\alpha_n = \frac{0.01\,\phi\,(10 - V_{sh})}{\exp\Big(\frac{10 - V_{sh}}{10}\Big) - 1}, \quad \beta_n = 0.125\,\phi\,\exp\Big(-\frac{V_{sh}}{80}\Big),$$

$$\alpha_m = \frac{0.1\,\phi\,(25 - V_{sh})}{\exp\Big(\frac{25 - V_{sh}}{10}\Big) - 1}, \quad \beta_m = 4\phi\,\exp\Big(-\frac{V_{sh}}{18}\Big),$$

$$\alpha_h = 0.07\phi\,\exp\Big(-\frac{V_{sh}}{20}\Big), \quad \beta_h = \frac{\phi}{\exp\Big(\frac{30 - V_{sh}}{10}\Big) + 1}.$$

Here $\phi = 3^{\frac{T-3.3}{10}}$ where T is the temperature, which is assumed to be 22^oC. The factor γ in equation (2.7) allows for the adjustment of the channel densities. Following values in [25], we use increased densities with $\gamma = 2.5$.

We will simulate the activation of a cluster of synapses by applying current to all spines in an activation region $X_o \le X \le X_o + \Delta X$. The expression for the synaptic current is given by

$$I_{syn}(X,t) = g_{syn}(X,t)(V_{sh} - V_{syn}) \tag{2.11}$$

where V_{syn} is the synaptic reversal potential and g_{syn} is a brief synaptic conductance generated by an $\alpha-$function given by

$$g_{syn}(X,t) = \begin{cases} g_p \dfrac{t}{t_p} e^{1-\frac{t}{t_p}}, & X_o \le X \le X_o + \Delta X, \quad t \in [0,p], \\ 0, & \text{otherwise}, \end{cases} \tag{2.12}$$

and $g_{syn}(X, t + kp) = g_{syn}(X,t)$ for $k = 1, 2, \ldots$. Here g_p is the peak synaptic conductance, t_p is the time required to reach the peak after synaptic activation, and p is the period for synaptic activation at a set frequency.

2.3. **Calcium concentration, stem resistance, and spine density.** Since the potential in the spine head increases with the increase in the synaptic activity, it is convenient to use the spine stem current defined in equation (2.1) as a measure of the electrical activity between the spine head and the dendritic base [26, 16]. If the potential in the spine head is higher than the potential in the dendrite, then $I_{ss} > 0$, and the current will flow from the spine head to the dendrite. Similarly, if

the potential in the spine head is less than the potential in the dendrite then $I_{ss} < 0$ and the current will flow from the dendrite to the spine head. If $I_{ss} = 0$, no current will pass through the spine stem.

The change in intraspine calcium is dependent on activity and is given by

$$\frac{\partial C_a}{\partial t} = -\epsilon_1(C_a - C_{min}) + \frac{1}{\kappa_c}|I_{ss}|. \tag{2.13}$$

Here, ε_1 is the rate constant for C_a decay due to calcium extrusion from the spine head (measured in ms^{-1}). κ_c (measured in $pA \cdot ms/nM$) is a scale factor that associates electrical activity, as measured by $|I_{ss}|$, with an increase in calcium. In the absence of activity ($I_{ss} = 0$), calcium will decay slowly to its minimum value, C_{min}. Observe that the change in calcium is constrained to vary with the potential difference between the spine head and the dendritic base which will increase in response to the increase in the spine head potential due to excitatory synaptic input. This is consistent with both calcium entry to the spine head that is associated with synaptic activity and also calcium entry through voltage-dependent ion channels. More detailed models for the calcium handling in the spine are possible but are not presented here.

We also need equations for the changes in dendritic spine density and stem resistance which are both mediated by the concentration of calcium. As reviewed in [24], a moderate and transient increase in calcium will cause elongation of spines and increases in spine density; however, if the amount of calcium is too low or too high, spines will start shrinking and eventually disappear, as summarized in the schematic in Figure 1. Thus, the equation for the change in spine density in the model is given by

$$\frac{\partial \bar{n}}{\partial t} = -\epsilon_3 \left(\frac{C_a}{C_{min}} - 1\right)\left(\frac{C_a}{C_1} - 1\right)\left(\frac{C_a}{C_2} - 1\right)\left(1 - \frac{\bar{n}}{\bar{n}_{max}}\right)(\bar{n} - \bar{n}_{min}). \tag{2.14}$$

Similarly, we add an equation for the change in the spine stem resistance R_{ss}, which is also mediated by the calcium concentration and is given by

$$\frac{\partial R_{ss}}{\partial t} = -\epsilon_2 \left(\frac{C_a}{C_{min}} - 1\right)\left(\frac{C_a}{C_1} - 1\right)\left(\frac{C_a}{C_2} - 1\right)\left(1 - \frac{R_{ss}}{R_{max}}\right)(R_{ss} - R_{min}). \tag{2.15}$$

Here, C_1 and C_2 are lower and upper threshold values for the effects of calcium in the spine head on the density and structure of spines. Equations (2.14) and (2.15) imply that the spine density $\bar{n}$ and the spine stem resistance R_{ss} will decay if the calcium level is either too low (i.e., below C_1) or too high (i.e., above C_2). The values of the parameters used in the model are summarized in Table 1. Note that ϵ_1 small ensures that the rate of change in calcium is slow relative to the changes in the membrane potential which occur on a millisecond time scale. Further, ϵ_2 and ϵ_3 are several orders of magnitude smaller than ϵ_1, since changes in spine length and spine density occur on a time scale of seconds to hours. Exact values for these parameters influence the time scales for the dynamics of the model but do not affect the overall behavior as long as these relative relationships are maintained.

2.4. **Analysis of slow variables.** Note that the forms of equations (2.14) and (2.15) have identical dependence on calcium; thus, the spine stem resistance and the spine density will have similar monotonic features as functions of t due to the activity-dependent changes in Ca over time. Therefore, for this analysis we focus our attention on the two equations (2.13) and (2.14) for Ca and $\bar{n}$; results for R_{ss} will be similar to those for $\bar{n}$. The only dependence between the subsystem defined

by (2.13) and (2.14) and the rest of the model is through the function I_{ss}. In what follows, we consider the dynamics of this subsystem where we treat I_{ss} as a fixed parameter which we call I_{ss}^*.

We can easily determine the Ca nullcline

$$Ca = C_{min} + \frac{I_{ss}^*}{\epsilon_1 \kappa_c} = C^*, \tag{2.16}$$

and the $\bar{n}$ nullclines

$$Ca = C_{min}, \quad Ca = C_1, \quad Ca = C_2, \quad \bar{n} = \bar{n}_{min}, \quad \bar{n} = \bar{n}_{max}.$$

A schematic depicting the steady states at the intersections of these nullclines is shown in Figure 2. For most values of I_{ss}^*, the system has two steady states, $(Ca^*, \bar{n}_{max})$ and $(Ca^*, \bar{n}_{min})$. By using the Jacobian to perform a linearization about these fixed points, it is easy to show that for $C_{min} < C^* < C_1$ and for $C^* > C_2$, the steady state $(Ca^*, \bar{n}_{max})$ is a saddle node and the steady state $(Ca^*, \bar{n}_{min})$ is a nodal sink. On the other hand, for $C_1 < C^* < C_2$, $(Ca^*, \bar{n}_{max})$ is a nodal sink and $(Ca^*, \bar{n}_{min})$ is a saddle node. When I_{ss}^* takes on values such that $Ca^* \in \{C_{min}, C_1, C_2\}$, the Ca nullcline will coincide with one of the $\bar{n}$ nullclines, resulting in an infinite number of stable steady states. These results are summarized in Figure 3. Note that in the full model, initial conditions are constrained so that $\bar{n}(0) \in [n_{min}, n_{max}]$, $R_{ss} \in [R_{min}, R_{max}]$, and $Ca(0) > C_{min}$. Therefore, we conclude that when the the calcium level in the spine head is in the range between C_1 and C_2, R_{ss} and $\bar{n}$ will increase to attain their maximum values R_{max} and $\bar{n}_{max}$ respectively. Otherwise, they will decreases slowly toward their minimum values R_{min} and $\bar{n}_{min}$.

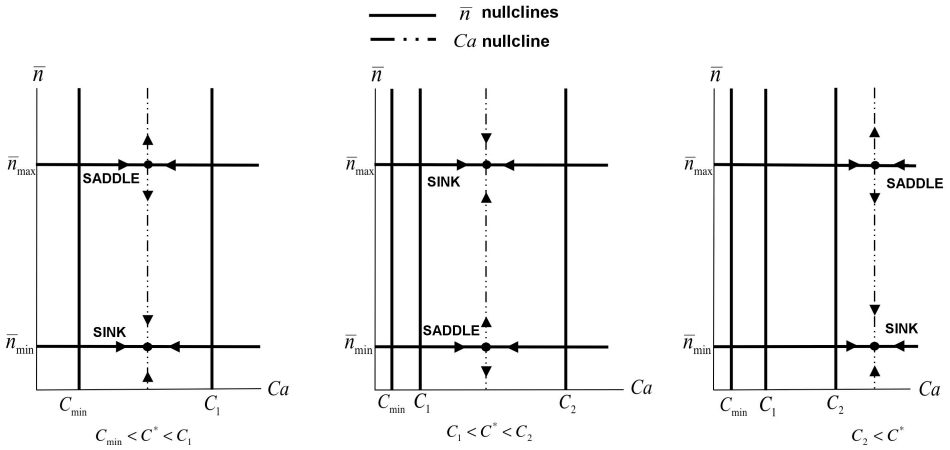

FIGURE 2. Schematic of the possible steady states for the slower subsystem and their dependence on parameter I_{ss}^*.

3. **Simulation results.** To improve computational efficiency we perform simulations using a spectral collocation method for the spatial discretization. Thus, simulation results are computed at spatial locations

$$X_i = -\frac{L/2}{cos(\pi/n)} cos(i\pi/n) + L/2$$

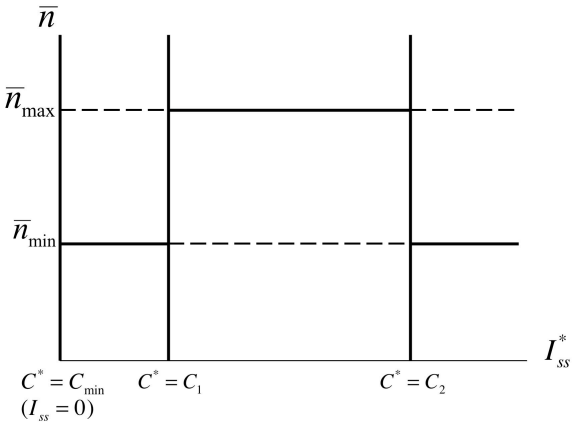

FIGURE 3. Schematic of the bifurcation diagram depicting the stability of all possible steady states for the slower subsystem as a function of I_{ss}^*.

where $n = 32$. For more details see Baer et al. [1].

Initially, we use simulations to explore how the model responds to local activity of different frequencies. Figure 4 demonstrates the effects of changes in Ca on the spine structure and density. For these simulation results, the initial stem resistance of all spines is 300 $M\Omega$, and the initial value for the spine density is 35 spines per unit of electrotonic length. The parameter values are described in Table 1. $\Delta X = 0.2$, so that the dendritic branch receives synaptic input on all spines in a small area at one end of the branch. Spines are activated repetitively at a set frequency, and each resulting post-synaptic action potential or spike results in an increase in Ca. For the 2 Hz stimulus (every 500 ms) shown in Panel A, the activity in the spine head is low, resulting in little accumulation of calcium. The calcium level stays below the lower threshold value ($C_1 = 30$), so there is a slow decrease in spine density. The shape of the curve demonstrating changes in R_{ss} is identical to that of the solution for $\bar{n}$; for example, when $\bar{n}$ decreases, there is also a decrease in R_{ss}. Thus, low-frequency stimulation also corresponds to shrinkage of existing spine. At the location depicted in Figure 4 ($X \approx 0.1$) both $\bar{n}$ and R_{ss} eventually approach their minimal values. For the 50 Hz stimulus (every 20 ms), the high level of activity in the spine head causes calcium to accumulate as shown in Panel B. The Ca level crosses the lower threshold, resulting in an increase in $\bar{n}$ and R_{ss} that corresponds to elongation of existing spines and formation of new spines. At location $X \approx 0.1$, both $\bar{n}$ and R_{ss} eventually approach their maximal values.

Now consider the local effects of the different levels of activity that result from synaptic inputs of additional frequencies, as demonstrated in Figure 5. Initial conditions and parameters are the same as those for the simulations depicted in Figure 4. Again, we consider the output at location $X \approx 0.1$ in the middle of the input region. Solution curves are labeled on the right with the frequency of the associated stimulus. As shown in Figure 4, the 2 Hz stimulus results in a slow decrease in spine density ($\bar{n} = 34.75$ at time $t = 2500ms$) at the synaptic input site. However, the 10 Hz stimulus results in an accumulation of Ca that remains in the region $30 < Ca < 300$, so that the spine density increases. As mentioned above, increases

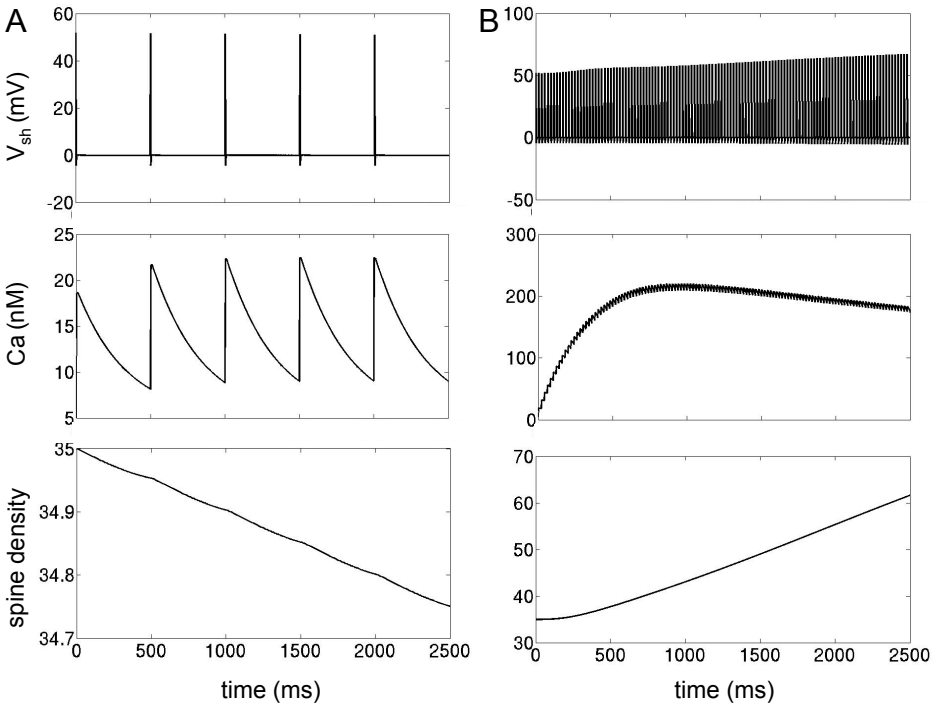

FIGURE 4. Simulation results for a 2 Hz (Panel A) and a 50 Hz (Panel B) stimulus lasting for 2500 ms for initial values of $\bar{n} = 35$ (≈ 2 spines/$10\mu m$) and $R_{ss} = 300$ $M\Omega$. Results are shown for the middle of the input site at $X \approx 0.1$.

in spine density are accompanied by increases in R_{ss} that represent spine elongation. These changes are more pronounced for the 50 Hz stimulus ($\bar{n} = 61.6$ at time $t = 2500$ ms). For the 100 Hz stimulus where spines in the input region are activated every 10 ms, Ca quickly accumulates to a level that exceeds the upper threshold for high-frequency pruning, $C_2 = 300$. Pruning and spine shrinkage occur which lead to a decrease in activity and subsequent decay of Ca. When the Ca concentration falls below the upper threshold, the spine density (and R_{ss}) begin to increase, leading to a return to activity in the spine head and accumulation of Ca. This process repeats, displaying a damped oscillation.

To further demonstrate the different effects of low-frequency and high-frequency stimuli that lead to pruning, consider the changes in spine density outside the region of synaptic input. Figure 6 demonstrates the changes along the dendritic branch for the 2 Hz stimulus discussed above (and shown in Figures 4 and 5). For the 2 Hz stimulus, the extremely low levels of activity slowly lead to a loss of spines and spine shrinkage along the length of the dendritic branch as shown in Figure 6. At all locations, both $\bar{n}$ and R_{ss} eventually approach their minimal values. However, for the 100 Hz stimulus, the rapid accumulation of calcium in the region

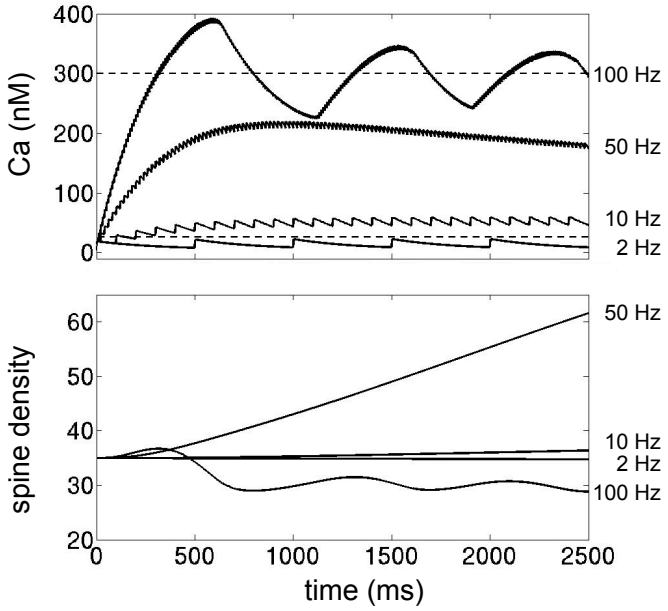

FIGURE 5. Simulation results for stimuli of four different frequencies lasting for 2500 ms. Initial values and parameters are the same as for Figure 4. Results are shown for the middle of the synaptic input region at $X \approx 0.1$. Top panel shows values of Ca, and bottom panel shows values for $\bar{n}$. Labels on the right side of both panels indicate the stimulus frequency associated with each curve. Spines are periodically activated at 2 Hz (every 500 ms), 10 Hz (every 100 ms), 50 Hz (every 20 ms) or 100 Hz (every 10 ms). Dashed lines indicate values of C_1 (lower) and C_2 (upper).

of synaptic input causes the spine density in that region to decrease quickly, leading to a decrease in the output of the branch as shown in Figure 5. At nearby locations along the dendritic cable, for example at $X \approx 2.0$, the decrease in activity ensures that the accumulated calcium stays below the critical level of $C_2 = 300$ so that the spine density continues to increase and the spines continue to elongate as shown in Figure 7. As in [27], we find that for some frequencies (e.g. 10 Hz) there are some locations where the calcium settles into a steady-state oscillation that averages one of the critical values such as $C_1 = 30$. In this case, R_{ss} and $\bar{n}$ approach values other than R_{max} or R_{min}.

A burst of high-frequency stimulation can reduce the dendritic output when spines shorten and spine density decreases, as shown in Figure 8. In this figure, a low-frequency input of 10 Hz is followed, at $t = 500\ ms$, by a high-frequency 125 Hz input. During the high-frequency input, Ca accumulation (Panel C) leads to spine pruning (Panel E) and spine shortening (Panel D). This causes action potential generation to fail in the input region due to too few channels (low $\bar{n}$) and increased dendritic load (low R_{ss}). Outside of the input region, there is the expected decrease in dendritic output as shown in Panel B. This decrease in output continues when the stimulus switches back to a low-frequency input at time $t = 1500\ ms$. However,

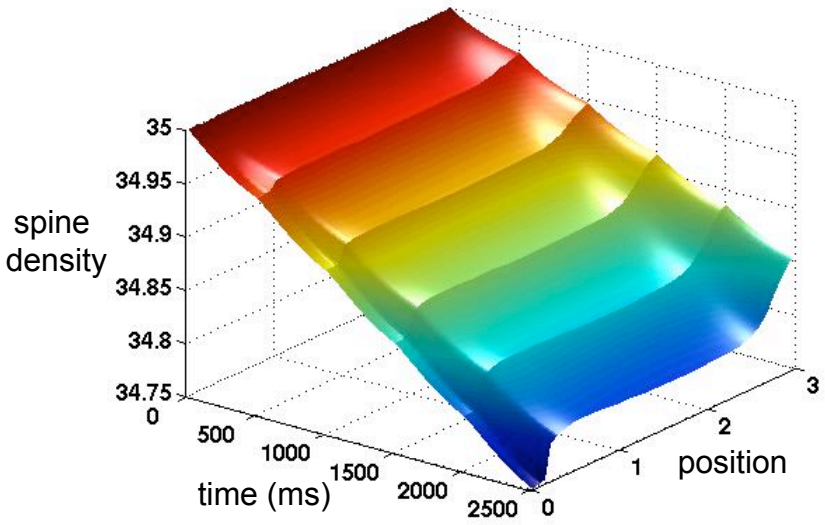

FIGURE 6. Simulation results for 2 Hz stimulus lasting for 2500 ms. Initial values and parameters are the same as for Figures 4 and 5. Changes in $\bar{n}$ are shown at all positions along the dendritic branch ($X = 0$ to $X = 3$).

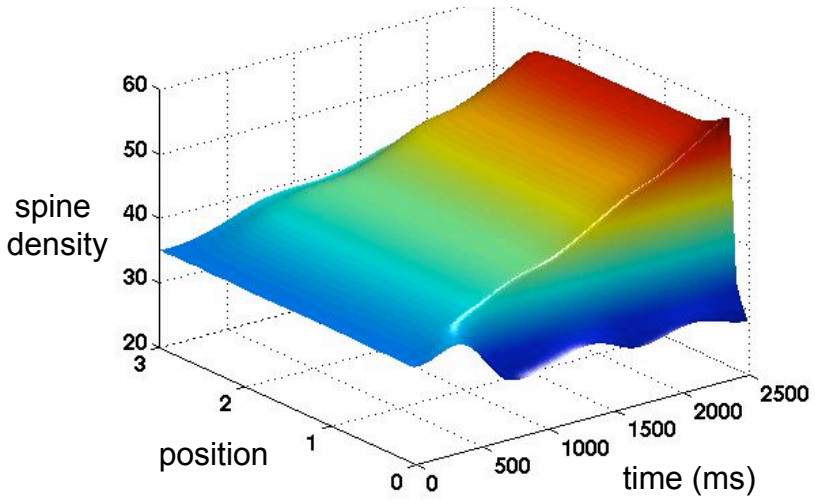

FIGURE 7. Simulation results for 100 Hz stimulus lasting for 2500 ms. Initial values and parameters are the same as for Figures 4 and 5. Changes in $\bar{n}$ are shown at all positions along the dendritic branch ($X = 0$ to $X = 3$).

eventually action potential generation and propagation resume since $Ca > 30\ nM$ and R_{ss} and $\bar{n}$ are increasing.

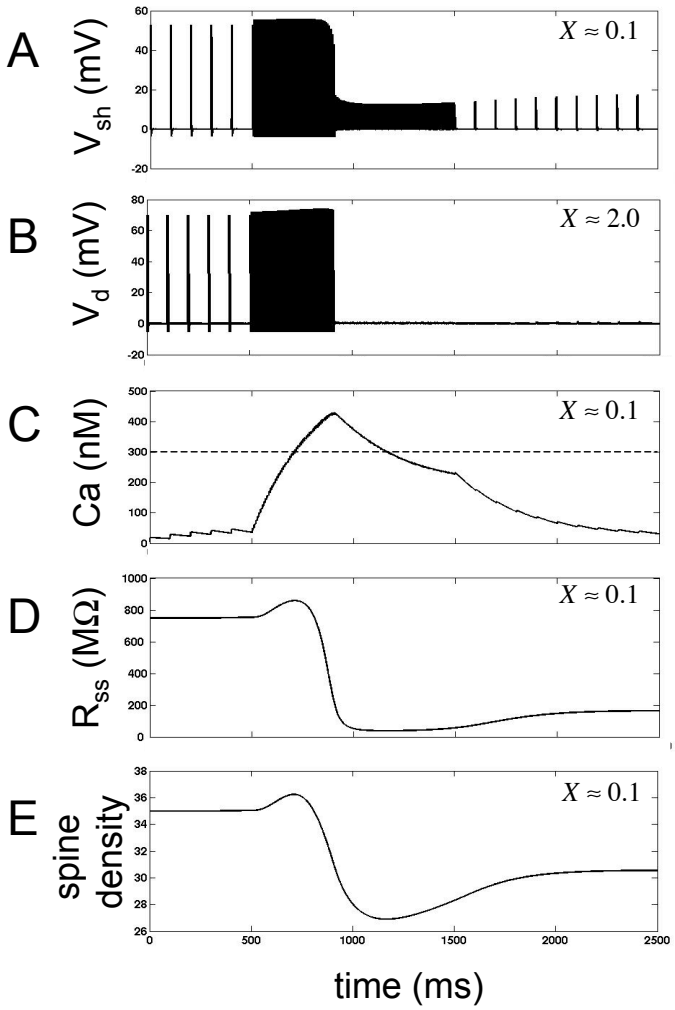

FIGURE 8. Simulation results for a 10 Hz stimulus lasting 500 ms followed by a 125 Hz stimulus for 1000 ms with a 10 Hz stimulus for the remainder of the simulation. Initial values and parameters are the same as for Figures 4 through 7, except that the initial value of $R_{ss} = 750\ M\Omega$. A: V_{sh} is shown at location $X \approx 0.1$. B: V_d is shown for $X \approx 2.0$. C: During the 125 Hz stimulus, Ca accumulates and exceeds the threshold for spine pruning and shrinking indicated by the dashed line. D and E: Both $\bar{n}$ and R_{ss} decrease during periods when $Ca > 300\ nM$. Note the decrease in the peak membrane potential in the spine head and the decrease in dendritic output after spine pruning and shortening in the region of synaptic input.

Clearly, these results depend critically on the values of C_1 and C_2. Figure 9 shows simulation results for a 40 Hz stimulus lasting 2500 ms for a higher value of C_1 ($C_1 = 100\ nM$). Other initial values and parameters are the same as for

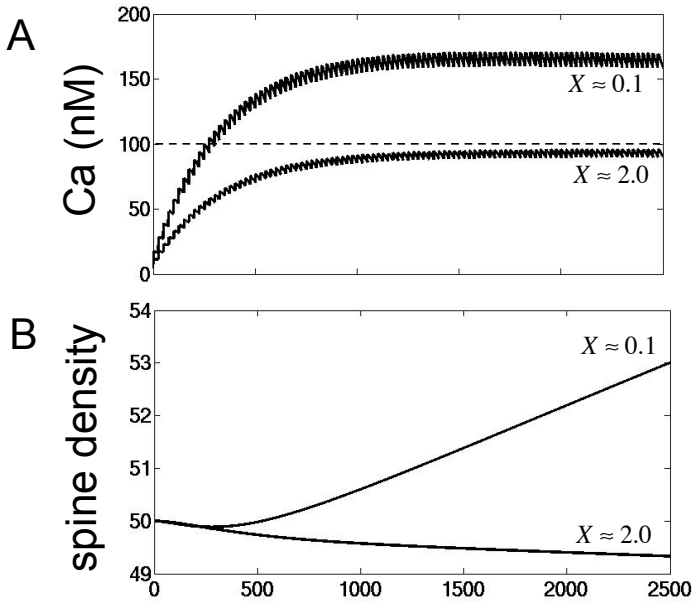

FIGURE 9. Simulation results for a 40 Hz stimulus lasting 2500 ms. Initial values and parameters are the same as for Figures 4 through 7 except that the initial spine density is 50 spines per unit electrotonic length, and $C_1 = 100$. In the region of synaptic input ($X \approx 0.1$), Ca accumulates and $C_1 < Ca < C_2$ so that R_{ss} and $\bar{n}$ increase as shown in Panel B. However, away from the input site ($X \approx 2.0$), $Ca < C_1$ so that R_{ss} and $\bar{n}$ decrease causing propagation failure.

Figures 4 through 7, except that the initial spine density is 50 spines per unit electrotonic length. In the region of synaptic input ($X \approx 0.1$), Ca accumulates and $C_1 < Ca < C_2$ (Panel A), so that R_{ss} and $\bar{n}$ increase (Panel B). However, even with a high initial spine density, there are regions away from the input site ($X \approx 2.0$) where $Ca < C_1$ (Panel A), forcing R_{ss} and $\bar{n}$ to decrease (Panel B), which promotes propagation failure.

4. **Discussion.** In these simulations, we investigated how localized synaptic activity might lead to activity-dependent changes in spine density and stem length and the subsequent effects on neighboring unstimulated spines and the output of the dendritic branch. We showed that for low-frequency stimuli like those associated with LTD, the model exhibits localized reductions in spine density as well as decreases in spine stem length. In contrast, high-frequency stimuli like those associated with LTP result in increases in spine density and spine stem length over most of the branch. For excitotoxicity, such as extremely high levels of activity due to seizures, the model exhibits reductions in spine density and stem length in the region of synaptic input. This can lead to a dramatic decrease in the output of the dendritic branch. However, these high levels of activity result in higher levels of calcium throughout the dendritic branch, so that nearby regions can exhibit an

increase in spine density and stem length if the calcium level in that region is below C_2. Verzi et al. [27] obtain the same result for high spine stem resistances. However, in their stem restructuring model with constant spine density, high-frequency stimuli have minimal effects on dendritic output for high spine densities and low spine stem resistance. Because the model presented here links calcium levels to both spine density and spine structure, the decrease in dendritic branch output for high-frequency stimuli is independent of the initial conditions for $\bar{n}$ and R_{ss}.

As discussed in [27], one important question is whether there are frequencies that give rise to an equilibrium value of R_{ss} that is different from R_{max} and R_{min}. For this model, stimulus frequencies that lead to an equilibrium value for R_{ss} also lead to an equilibrium value for $\bar{n}$. These steady states suggest the possibility that under some circumstances, average spine lengths and densities reflect the average frequencies of synaptic input.

Earlier continuum models link changes in spine density to activity through I_{ss} [27, 1]. In contrast, our model relies on the local calcium concentration, which in turn depends on activity. This allows us to include concepts from [24] that describe associations between calcium levels and structural changes based on experimental data. One major difference between the model presented here and earlier continuum modeling studies is the addition of spine pruning and shrinkage for low-frequency inputs. This leads to the observation that for some inputs, the C_1 threshold determines whether activity remains local to the activation region or propagates. The next step in these modeling studies will be to incorporate more realistic calcium dynamics, including calcium buffering and calcium-induced calcium release from internal stores, which has been demonstrated experimentally [8].

Acknowledgments. We thank Z. Jackiewicz for his contributions to the numerical techniques used here and W. Tyler for helpful discussions of experimental studies. We would also like to thank the anonymous reviewers for their suggestions, which resulted in improvements to the manuscript. Parts of this work appeared previously in abstract form.

REFERENCES

[1] Baer, S. M., S. Crook, M. Dur-e-Ahmad and Z. Jackiewicz: Numerical solution of calcium-mediated dendritic branch model. *submitted*.

[2] Baer, S. M. and J. Rinzel: Propagation of dendritic spikes mediated by excitable spines: A continuum theory. *Journal of Neurophysiology*, 1991, 65:874-890.

[3] Bliss, T. V. P. and G. L. Collingridge: A synaptic model of memory: Long term potentiation in the hippocampus. *Nature*, 1993, 361:31-39.

[4] Calabrese, B., M. S. Wilson and S. Halpain: Development and regulation of dendritic spine synapses. *Journal of Physiology*, 2006, 21:38-47.

[5] Collin, C., K. Miyagushi and M. Segal: Dendritic spine density and LTP induction in cultured hippocampal slices. *Journal of Neurophysiology*, 1997, 77:1614-1623.

[6] El-Husseini, A. E., E. Schnell, D. M. Chetkovich, R. A. Nicoll and D. S. Bredt: PSD-95 Involvement in maturation of excitatory synapses. *Science*, 2000, 290:1364-1368.

[7] Engert, F. and T. Bonhoeffer: Dendritic spine changes associated with hippocampal long-term synaptic plasticity. *Nature*, 6 MAY 1999, 399:66-70.

[8] Harris, K. M.: Calcium from internal stores modifies dendritic spine shape. *Proceedings of the National Academy of Sciences USA*, 1999, 96:12213-12215.

[9] Hayashi, Y. and A. K. Majewska: Dendritic spine geometry: Functional implication and regulation. *Neuron*, 2005, 46:529-532.

[10] Hering, H. and M. Sheng: Dendritic spines: Structure, dynamics and regulation. *Nature Reviews*, December 2000, 2:880-888.

[11] Hodgkin, A. L. and A. F. Huxley: A quantitative description of membrane current and its application to conduction and excitation in nerve. *Journal of Physiology*, 1952, 117:500-544.
[12] Holcman, D., Z. Schuss and E. Korkotian: Calcium dynamics and dendritic spines and spine motility. *Biophysical Journal*, July 2004, 87:81-91.
[13] Holthoff, K., D. Tsay and R. Yuste: Calcium dynamics of spines depend on their dendritic location. *Neuron*, January, 2002, 33:425-437.
[14] Jaffe, D. B., S. A. Fisher and T. H. Brown: Confocal laser scanning microscopy reveals voltage-gated calcium signals within hippocampal dendritic spines. *Journal of Neurobiology*, 1994, 25:220-223.
[15] Korkotian, E. and M. Segal: Fast confocal imaging of calcium released from stores in dendritic spines. *European Journal of Neuroscience*, 1998, 10:2076-2084.
[16] Kuske, R. and S. M. Baer: Asymptotic analysis of noise sensitivity in a neuronal burster. *Bulletin of Mathematical Biology*, 2002, 64:447-481.
[17] Lamprecht, R. and J. LeDoux: Structural plasticity and memory. *Nature Reviews Neuroscience*, January 2004, 5:45-54.
[18] Lynch, G., J. Larson, S. Kelso, G. Barrionuevo and F. Schotter: Intracellular injection of EGTA blocks induction of hippocampal long term potentiation. *Nature*, 1983, 305:719-721.
[19] Majewska, A., E. Brown, J. Ross and R. Yuste: Mechanisms of calcium decay kinetics in hippocampal spines: Role of spine calcium pumps and calcium diffusion through the spine neck in biochemical compartmentalization. *Journal of Neuroscience*, 2000. 20:1722-1734.
[20] Maletic-Savatic, M., R. Malinow and K. Svoboda: Rapid dendritic morphogenesis in CA1 hippocampal dendrites Induced by synaptic activity. *Science*, 19 March 1999, 1923-1927.
[21] Muller, D., A. Gahwiler, L. Rietschin and S. M. Thompson: Reversible loss of dendritic spines and altered excitability after chronic epilepsy in hippocampal slice cultures. *Proc. Natl. Acad. Sci. USA*, 1993, 90:257-261.
[22] Nagerl, U. V., N. Eberhorn, S. B. Cambridge and T. Bonhoeffer: Bidirectional activity-dependent morphological plasticity and hippocampal neurons. *Neuron*, 2004, 44:759-767.
[23] Nimchinsky, E. A., B. L. Sabatini and K. Svoboda: Structure and function of dendritic spines. *Annual Reviews Physiology*, 2002, 64:313-353.
[24] Segal, M., E. Korkotian and D. D. Murphy: Dendritic spine formation and pruning: Common cellular mechanisms? *Trends in Neuroscience*, 2000, 23:53-57.
[25] Segev, I. and W. Rall: Computational study of an excitable dendritic spine. *Journal of Neurophysiology*, 1988, 60:499-523.
[26] Wu, H.-Y. and S. M. Baer: Analysis of excitable dendritic spine with an activity-dependent stem conductance. *Journal of Mathematical Biology* 1998, 36:569-592.
[27] Verzi, D.W, M. B. Rheuben and S. M. Baer: Impact of time-dependent changes in spine density and spine shape on the input-output properties of a dendritic branch: A computational study. *Journal of Neurophysiology*, 2005, 93:2073-2089.
[28] Yuste, R. and T. Bonhoeffer: Morphological changes in dendritic spines associated with long-term synaptic plasticity. *Annual Reviews in Neuroscience*, 2001, 24:1071-89.

Received on February 12, 2007. Accepted on June 21, 2007.

E-mail address: sharon.crook@asu.edu.
E-mail address: ahmad@mathpost.asu.edu.
E-mail address: baer@math.asu.edu.